Green Synthesis of Flower-Shaped Copper Oxide and Nickel Oxide Nanoparticles via *Capparis decidua* Leaf Extract for Synergic Adsorption-Photocatalytic Degradation of Pesticides

Amna Iqbal [1,2], Atta ul Haq [1], Gabriel Antonio Cerrón-Calle [2], Syed Ali Raza Naqvi [1], Paul Westerhoff [2] and Sergi Garcia-Segura [2,*]

[1] Department of Chemistry, Government College University Faisalabad, Punjab 38000, Pakistan; 2016-gcuf-000028@gcuf.edu.pk (A.I.); attaulhaq@gcuf.edu.pk (A.u.H.); draliraza@gcuf.edu.pk (S.A.R.N.)

[2] Nanosystems Engineering Research Center for Nanotechnology-Enabled Water Treatment, School of Sustainable Engineering and the Built Environment, Arizona State University, Tempe, AZ 85287-3005, USA; gcerron@asu.edu (G.A.C.-C.); p.westerhoff@asu.edu (P.W.)

* Correspondence: sergio.garcia.segura@asu.edu

Abstract: Green manufacturing of catalysts enables sustainable advanced oxidation processes and water treatment processes for removing trace contaminants such as pesticides. An environmentally friendly biosynthesis process produced high-surface-area CuO and NiO nanocatalysts using phytochemicals in the *Capparis decidua* leaf extract, which served as a reductant and influenced catalyst shape. *Capparis decidua* is a bushy shrub, widely distributed in dry and arid regions of Africa, Pakistan, India, Egypt, Jordan, Sudan, Saudi Arabia. The synthesized CuO and NiO nanoparticles were characterized by UV-vis spectroscopy (UV-vis), field emission scanning electron microscopy (FESEM), energy-dispersive X-ray spectroscopy (EDS), Fourier transform infrared spectroscopy (FT-IR), and X-ray diffraction (XRD) and thermo-gravimetric analysis/differential thermal analysis (TGA/DTA). The produced nanoparticles were spherical and flower-like in shape and have a characteristic face-centered cubic structure of CuO and NiO. Biosynthesized catalysts were photoactive and degraded recalcitrant pesticide Lambda-cyhalothrin (L-CHT). Photocatalytic degradation of L-CHT was affected by the initial L-CHT concentration, solution pH levels between 5 and 9, and photocatalyst concentration. The L-CHT removal percentage attained by CuO photocatalyst (~99%) was higher than for NiO photocatalyst (~89%). The degradation of L-CHT follows a pseudo-first-order kinetic model, and the apparent rate constant (k_{app}) decreased from 0.033 min^{-1} for CuO to 0.0084 min^{-1} for NiO photocatalyst. The novel flower-shaped nanoparticles demonstrated high stability in water and recyclability for removing L-CHT pesticide contamination in water.

1. Introduction

To ensure food security and improved nutrition for all, it is necessary to protect crop production at higher yields. The use of pesticides contributes toward battling hunger worldwide by protecting crops from different insects. However, the use of certain pesticides is associated with hazardous effects to environmental health [1,2]. Sustainable agriculture should not only ensure food for all, but also protect the environment and human health [3]. The implementation of measures that remove pesticides from agricultural runoff is a must [4]. Several physical and chemical methods have been explored as possible decentralized water treatment technologies, such as filtration or ozonation [5,6]. Unfortunately, the high costs associated with these technologies are a major barrier to implementation in developing countries [5]. Thus, there is a need for an alternative, more economical method for the complete mineralization of pesticides into ecofriendly byproducts in the water [7,8]. Among the range of potential competing technologies available

to degrade organic pollutants, photocatalysis has emerged as a way to control pesticide residue because it competitiveness and it is not necessary to add other chemicals to water (e.g., hydrogen peroxide) [9,10].

Semiconductor metal-oxides have shown excellent photocatalytic properties, which can be exploited as affordable advanced oxidation processes (AOPs) for pesticide abatement [11,12]. Titanium dioxide catalysts have been widely studied as the gold standard material [13–15]. Solar light active photocatalysts can be easily deployed as decentralized water treatment technologies [16,17]. However, the recent incorporation of light-emitting diodes (LEDs) to the water treatment toolbox has opened a new avenue for light-driven processes by enabling the inexpensive use of UV-light sources [18,19]. Thus, different semiconductor materials are re-emerging as competitive alternatives of interest for such off-grid and decentralized applications [20,21]. Copper and nickel oxides nanoparticles are a promising class of photoactive nanomaterials in the scientific spotlight, due to their attractive properties. CuO and NiO have been identified as effective photocatalysts because of their ability to degrade a wide range of several organic pollutants with low cost, low toxicity, and high photostability [22,23]. NiO has a bandgap energy similar to TiO_2 of ~3.5 eV [24], whereas CuO has a lower bandgap of 1.2 eV [25].

Sustainable treatment approaches must consider the approach holistically, beyond the system level. Photocatalyst synthesis has to consider green and sustainable approaches to minimize environmental impact when considering the overall lifecycle of a treatment technology [26–28]. In recent decades, conventional metal oxide nanoparticle synthesis methods have relied on the use of hazardous chemicals and solvents plus energy-intensive approaches [29–32]. Novel biological synthesis routes are an exciting pathway to catalyze the transition to greener manufacturing strategies.

Bio-inspired methods for the synthesis of nanoparticles offer distinct advantages, because of the direct use of natural and biological resources through more simple, non-toxic biocompatible and inexpensive synthesis routes [33,34]. Among the bio-inspired methods, the green synthesis of metal oxide nanoparticles using plant extracts can be highlighted as a simple, economical, and eco-friendly method [35]. Plant extracts contain bioactive compounds such as phenols, ascorbic acid, flavonoids, polyphenolic, citric acid, alkaloids, terpenes, and reductase [36]. These biologically active compounds act as reducing and stabilizing agents, which help in the reduction in metal ion precursors and formation of desired nanoparticle structures [37]. The synthesis of metal oxide nanoparticles is attracting attention because of the possibility of transitioning to the use of green and sustainable sources. The synthesis of CuO nanoparticles can be used for different purposes. For example, *Adiantum lunulatum* was used to synthesize CuO to use as a plant defense booster [38], *Lantana camara* flower extract was used to enhance CuO catalytic and recyclability properties in an aza-Michael addition reaction [39], while *Caesalpinia bonducella* seed extract was used to synthesize a suitable CuO sensor for the electrochemical detection of riboflavin [40]. Other plant extracts were used to manufacture NiO nanoparticles. These include *Ananas comosus* leaf extract to develop NiO nanopowder to degrade polyethylene films [41], *Calendula officinalis* to develop NiO nanoparticles as chemotherapeutic supplement/drug to treat esophageal carcinoma [42], or *Nigella sativa* extract, which was used to develop NiO electrocatalytic nanoparticles active in the degradation of 4-nitrophenol [43].

In this research, we use *Capparis decidua* for the biosynthesis of CuO and NiO nanoparticles in an effortless, single-phase process. *Capparis decidua* is a member of the family *Capparidaceae* of plants and is also known locally as Karir, Caper, Han bag, Karyal, etc. [44]. It is a bushy shrub and is widely distributed in dry and arid regions of Africa, Pakistan, India, Egypt, Jordan, Sudan and Saudi Arabia [45]. In Cholistan, Pakistan, the floral buds are used as vegetables and pickles, and leaves are used as food for cattle. It has been reported that almost all of its parts have been used as traditional medicines (Greco-Arab, Ayurveda, Chinese, Tibb-e- Unani, etc.) and in the treatment of arthritis, alleviate cholera, urinary purulent discharges, constipation, cough, intermittent fevers, puffiness, toothache, asthma, dysentery, cardiac problems, soreness and skin diseases [44–47]. There is no previ-

ous research reporting the usage of a *Capparis decidua* plant extract for the preparation of CuO and NiO nanoparticles.

Lambda-cyhalothrin (L-CHT) is a type II pyrethroid insecticide used in agriculture, horticulture, forestry, and households to control pests and insects. Unfortunately, the widespread use of cyhalothrin in Pakistan has resulted in severe environmental pollution [48–50]. Several reports have shown that it is abundantly present in water resources [51–53] and it is susceptible to entering the trophic chain [54]. L-CHT is highly toxic to amphipods, aquatic invertebrates, fish, and mice [51,55–60]. Humans exposed to cyhalothrin via ingestion of food, inhalation, dermal contact, or drinking water can be exposed to deleterious and harmful effects [56,61]. The continuous and significant dose exposure to cyhalothrin in mammals may cause serious health effects such as genotoxicity, neurotoxicity, cytotoxicity, carcinogenicity, endocrine disruption, mutagenicity, damage reproduction cycle, and even childhood leukemia [50,62]. Due to its noxious and hazardous effects, L-CHT use has been banned in Canada and the US [63,64]. However, L-CHT is allowed and extensively used in Pakistan. Other countries worldwide use L-CHT to control plagues. Thus, there is an urgent need for effective strategies to remove cyhalothrin from the environment because it poses a serious threat to human health and the ecosystem.

In the present study, CuO and NiO nanoparticles using *Capparis decidua* leaf extract were synthesized by an eco-friendly method, and their photocatalytic activity was studied for signs of L-CHT degradation. The synthesized nanoparticles were characterized, and their photocatalytic capabilities were evaluated regarding the degradation of L-CHT as a target pollutant. The photocatalytic degradation of L-CHT was performed under the influence of various parameters, such as the effect of pH, catalyst dosage, initial concentration of L-CHT, to achieve optimum conditions for the degradation of L-CHT.

2. Results and Discussion

2.1. Photocatalytic Nanoparticles Synthesis and Characterization

The green synthesis of CuO and NiO nanoparticles was assessed by the rapid change in color of *Capparis decidua* leaf extract solution from light green to dark green and dark brown, within 5 min of the addition of $Cu(NO_3)_2 \cdot 3H_2O$ and $Ni(NO_3)_2 \cdot 6H_2O$, respectively. The formation and stability of CuO and NiO NPs were initially confirmed using UV−vis absorption spectroscopy. Figure 1 shows the drastic change in the absorbance spectra of *Capparis decidua* leaf extract when CuO and NiO NPs were formed in solution. Note the differential presence of peaks in maximum absorbance of CuO and NiO nanoparticles at 570 nm and 410 nm, respectively.

The surface morphology of synthesized CuO and NiO nanoparticles was analyzed using FE-SEM. FE-SEM images of Figure 2 show that the synthesized CuO and NiO nanoparticles predominantly have five to six petal flower-shaped structures, with the center of each flower having a cupola-shaped surface. In a recent study, FE-SEM images of *Solanum-lycopersicum*-mediated, synthesized iron nanoparticles (FeONPs) showed similar flower-like agglomerated structures [65], which were associated with the characteristic nano-structure of nanoparticles synthesized with plant extracts. Thus, we demonstrate that the formation of high-surface-area, flower-shaped structures is possible with copper and nickel, and not only iron. Nanoparticles synthesized following this green method attained a homogeneous size distribution with an average diameter of 900 nm for both metal oxides, CuO and NiO. These results suggest that phyto-fabrication through the use of plant extracts can introduce a high reproducible control of the size of synthesized metal-oxides. The EDX analysis of CuO nanoparticles showed characteristic peaks associated with copper at 0.93 keV, 8.04 keV and 8.91 keV, with relative intensities of 100:37:5, that correspond to transitions of Cu L_α, Cu K_α and Cu K_β, respectively. Meanwhile, the NiO nanoparticles showed characteristic peaks in Ni at 0.85 keV, 7.47 keV and 8.2 keV, with relative intensities of 100:69:10, that correspond to transitions of Ni L_α, Ni K_α and Ni K_β, respectively. This confirms that the phyto-fabricated nanoparticles were successfully synthesized. The peaks associated with C signal in both EDX spectra were attributed to remaining impurities of

organic plant extracts (e.g., flavonoids, polyphenol, proteins) on the nanoparticles. These results agree with the phyto-synthetic processes of CuO and ZnO from *Azadirachta indica* previously reported in the literature [66].
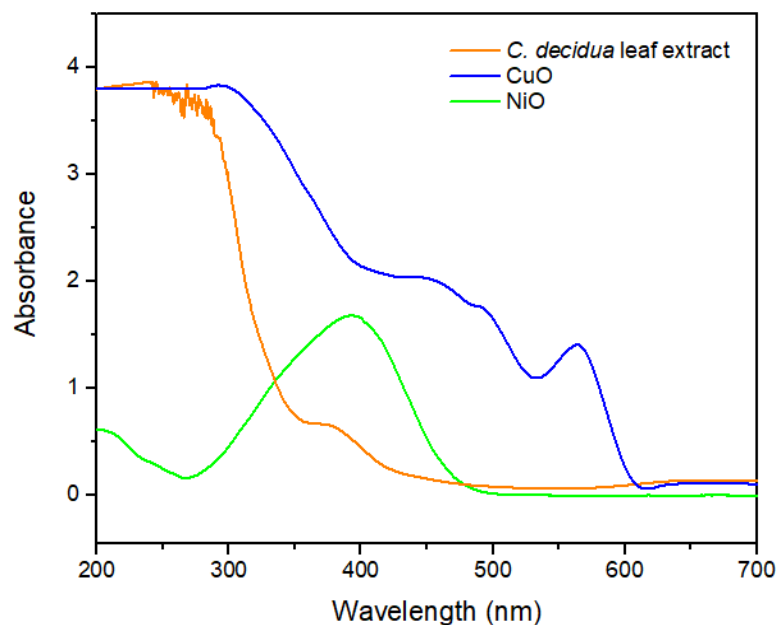

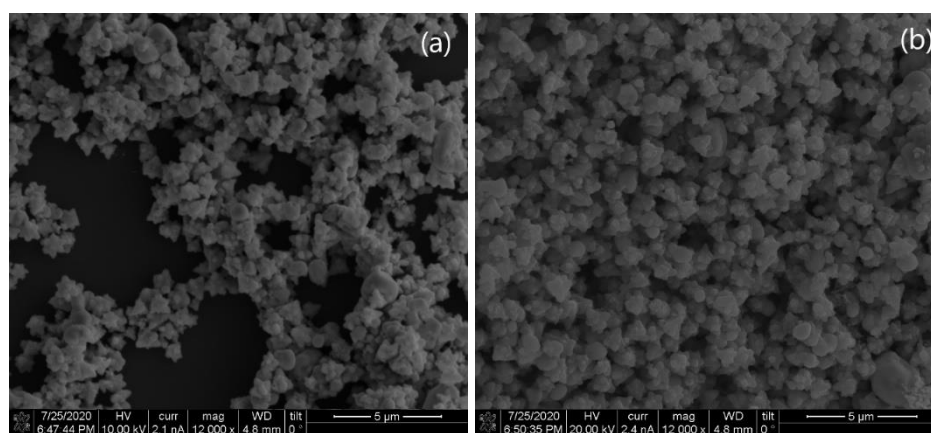**Figure 1.** UV–vis spectra of *Capparis decidua* leaf extract and CuO and NiO solutions.

**Figure 2.** FE-SEM images of CuO (**a**) and NiO (**b**) nanaoparticles.

The FTIR spectra of CuO and NiO nanoparticles synthesized using *Capparis decidua* leaf extract are shown in Figure 3. The FTIR allows for the identification of possible biomolecules responsible for the reduction and stabilization of CuO and NiO nanoparticles. The FTIR spectra of CuO nanoparticles (cf. Figure 3) shows a characteristic band at 508 cm^{-1} that indicates the stretching of Cu–O vibration. The peaks observed at 1043, and 1339 cm^{-1} can be assigned to C–O–C and C–N vibrations of the amide band of proteins, whereas the peaks at around 1505 and 2364 cm^{-1} are due to the presence of –COOH group and N–H stretching vibration in the amino acids of protein [67,68]. These results are in agreement with the EDX spectra that showed a carbon signal associated with organic compounds adsorbed as result of the synthesis process. The FTIR spectra analysis of NiO nanoparticles shown in Figure 3 also presents these coincident peaks, associated with the impurities previously discussed for CuO [69–71]. However, the NiO FTIR spectra show a characteristic peak at 848 cm^{-1}, which is an indication of Ni–O–Ni vibration. The small

absorption peaks at 3749 and 3756 cm^{-1} may be caused by the active hydrogen bond of water molecules adsorbed on CuO and NiO nanoparticles [69].
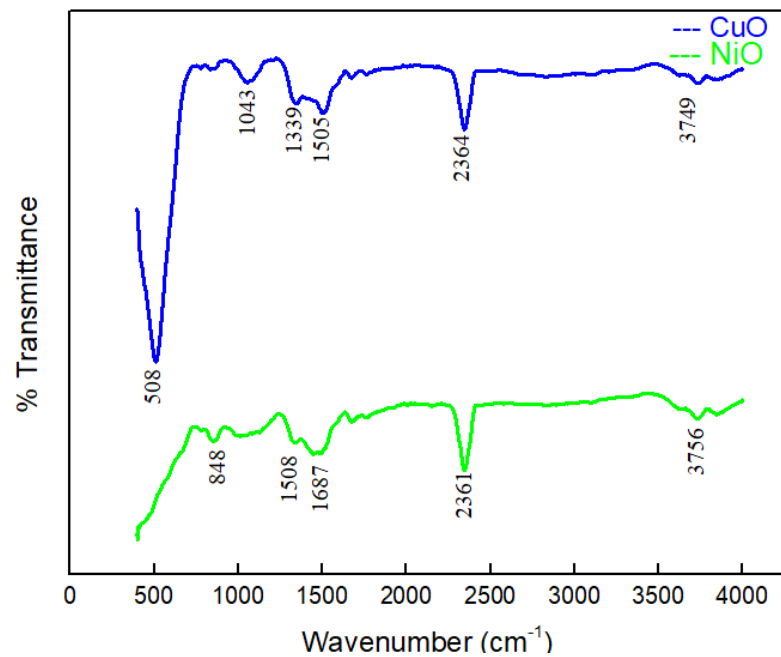
Figure 3. FTIR spectrum of CuO and NiO nanoparticles.

Figure 4 shows the XRD spectrum of CuO and NiO nanoparticles synthesized using *Capparis decidua* extract. The strong and sharp distinct diffraction peaks in CuO nanoparticles at 2θ = 35.53, 38.79, 48.72, 61.60, 66.09, and 68.11 degrees are associated with the (−111), (111), (−202), (200), (−113), and (202) crystalline planes of CuO monoclinic crystalline structure [72]. The XRD diffractogram of CuO agrees well with JCPDS card 01-080-1268, further confirming that copper oxide nanoparticles are crystalline [73].
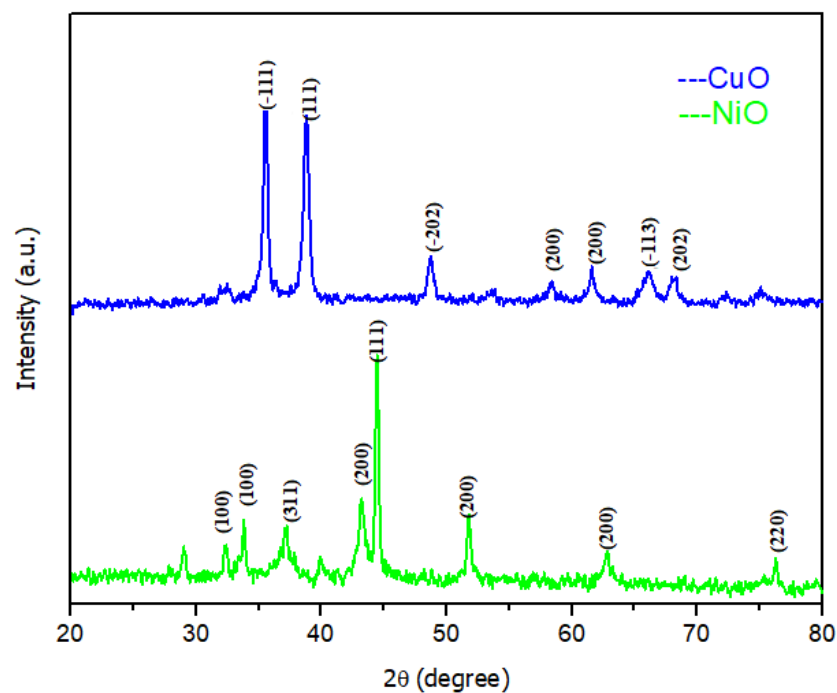
Figure 4. XRD pattern of CuO and NiO nanoparticles.

The intense peaks in NiO nanoparticles at 2θ = 32.4, 33.8, 37.25, 43.2, 44.45, 51.75, 62.95 and 76.35 degrees were associated with the (100), (100), (311), (200), (111), (200), (200) and (220) crystalline planes. Two high-intensity peaks were identified at 2θ = 43.2, 44.45 degrees. The XRD pattern was in accordance with JCPDS card 04-0835, confirming that NiO nanoparticles are crystalline and have a pure face-centered cubic phase structure [74,75]. The CuO and NiO nanoparticles have an average crystallite size of 11.23 nm and 16.75 nm, respectively, which were calculated using the classical Debye-Scherrer Equation (1)

$$D = \frac{0.9/\lambda}{\beta cos\theta},$$ (1)

where D is crystallite size, λ is the X-ray wavelength (0.1546 nm), β is the is the full width at half maximum of the peak in radians, and θ is the Bragg diffraction angle.

The thermal stability of phytochemical-synthesized NPs was investigated by TGA-DTA. Figure 5a depicts that CuO NPs lose about 10 wt% weight between 30 and 100 °C, due to the removal of moisture content. The gradual loss of mass observed between 100 and 600 °C for both CuO and NiO NPs was associated with the volatilization of plant extracts present in the nanoparticle powder. Then, CuO experienced nearly 27 wt% weight loss within 600–720 °C, corresponding to the combustion of organic matter (*Capparis decidua* extract) of the sample, which was observed in FTIR (see Figure 3). Figure 5b illustrates the TGA-DTA curve of NiO NPs. About 15 wt% weight loss was observed between 30 and 100 °C, which is associated with the removal of moisture content (similarly to the trend observed for CuO NPs). Then, a nearly 30 wt% weight loss was observed at 600–700 °C corresponding to combustion of organic matter (*Capparis decidua* extract). The remaining mass in both cases is characteristic of semiconductor oxides that cannot be thermally degraded.
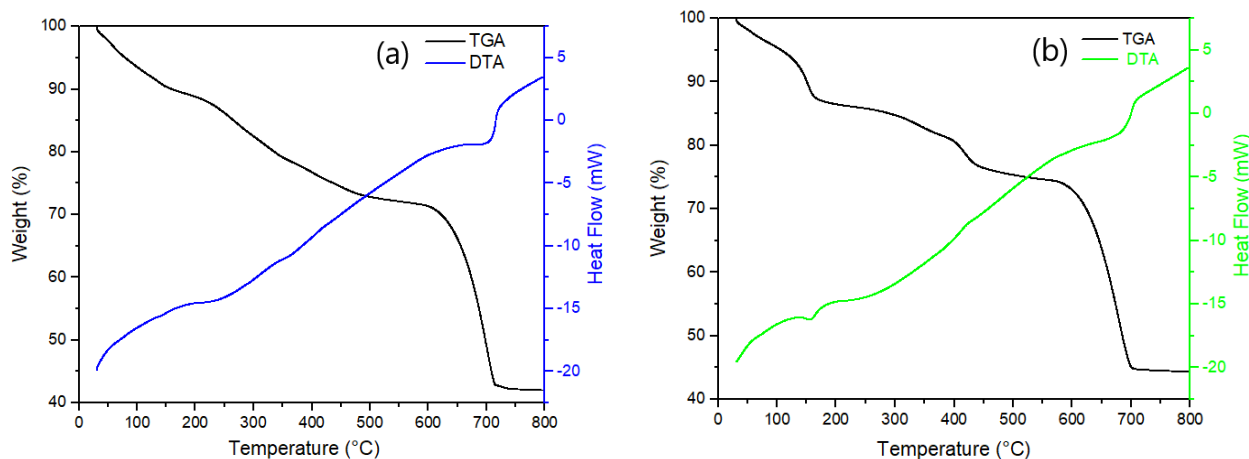

Figure 5. TGA-DTA of CuO (**a**) and NiO (**b**) nanoparticles.

2.2. Evaluating the Photocatalytic Activity of Phyto-Synthesized Nanoparticles

Semiconductor nanoparticles present photocatalytic activity when submitted to light irradiation of photons of energy which are equal or superior to the material bandgap. To evaluate the photocatalytic response of phytosynthetic flower-shaped nanoparticles of CuO and NiO, the removal of L-CHT was followed under a natural pH 7.0, but considering different operation conditions under dark conditions or UV irradiation, illustrated in Figure 6. Experiments conducted in the absence of a catalyst exposing L-CHT solutions to UV irradiation did not show an appreciable abatement of the pesticide (<10%) within 180 min of irradiation. This result suggests that L-CHT has high photostability, which is in agreement with its recalcitrant character and presence in natural conditions in rivers and lakes [49,51]. Experiments conducted in the dark but in the presence of 2 mg L^{-1} semiconductor nanoparticle showed the discrete abatement of L-CHT of 17% for CuO

and 11% for NiO after 180 min. It can be inferred that the removal of L-CHT was mostly associated with organics adsorption on the semiconductors. Semiconductor irradiation showed synergistic effects that resulted in an almost complete abatement of L-CHT by CuO in only 180 min. Conversely, a lower removal capability was assessed for NiO that only attained 77.27% degradation of L-CHT in 180 min. Both photosynthesized catalysts showed higher levels of removal than P25 TiO$_2$. It can be concluded that as-synthesized CuO petal-shape nanoparticles present a higher photoactivity for organics' abatement than NiO.
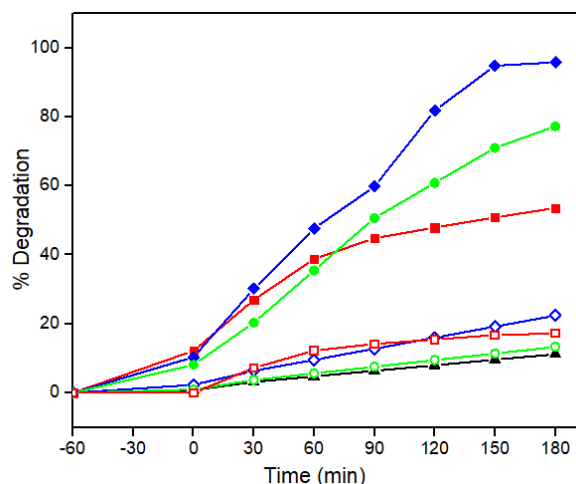
Figure 6. Degradation of 20 mg L^{-1} L-CHT at pH = 7 using 2 mg L^{-1} of photocatalyst (◆,◇) CuO, (●,○) NiO, and TiO$_2$ (■,□). Experiments were conducted under UV-light irradiation (filled symbols) or in the dark (empty symbols). Additionally, a blank experiment was conducted to evaluate the effect of (▲) direct photolysis.

2.3. Understanding the Impact of Operational Variables on Pesticide Removal

Operational conditions can affect the performance of photocatalytic treatments. One of the most relevant parameters is solution pH since it can modify the speciation of target pollutants and the surface charge of catalysts. The pesticide L-CHT does not have any functional group with acid-base properties. Thus, L-CHT speciation is not affected by pH changes, and it remains a neutral compound in a wide pH range. The effect of initial pH on the photocatalytic degradation of L-CHT by using CuO and NiO NPs was investigated by varying the initial pH from 5 to 9 at constant catalyst loading of (2 mg L^{-1}) and constant initial L-CHT concentration (20 mg L^{-1}), which are representative of the natural pH of agricultural run-off waters. Figure 7 shows the degradation efficiency of L-CHT by varying the initial pH. It has been observed that both catalysts (CuO and NiO) showed the highest degradation efficiency at pH 7. By using the CuO photocatalyst, the degradation efficiency of L-CHT was enhanced from 86% to 98% by increasing the initial pH from 5 to 7, and then decreasing it to 91.7 % at pH 9. However, by using the NiO photocatalyst, the degradation efficiency of L-CHT was enhanced from 63% to 77% by increasing the initial pH from 5 to 7, and then was intermediate (71%) at pH 9. Given the non-charged character of L-CHT, the lower degradation performance cannot be associated with electrostatic repulsion or attraction effects. The most common reactive oxygen species involved in the degradation of organic pollutants following photocatalytic processes are hydroxyl radical and superoxide radical [26,76,77]. Note that the reduction potential of reactive oxygen species is dependent on the pH; therefore, lower oxidation abilities are expected at a higher pH. The lower removal attained at a higher alkaline pH can be associated with the lower oxidation capabilities of reactive oxygen species at alkaline pH [78]. From this study, pH 7 was identified as an optimum pH for the degradation of L-CHT.
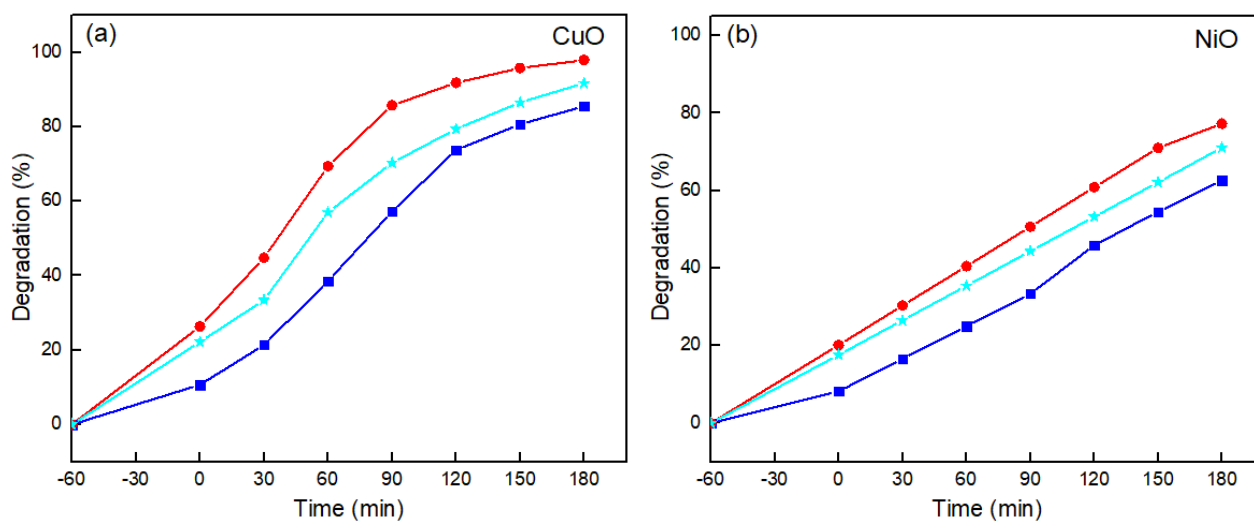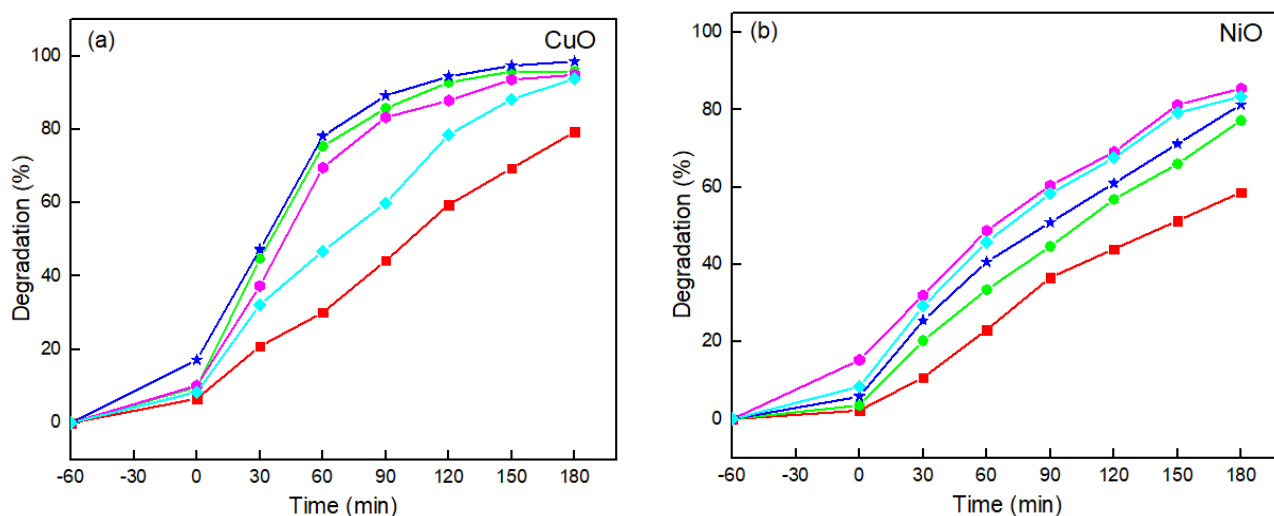
Figure 7. Effect of initial pH on the photocatalytic degradation of L-CHT using (**a**) CuO, (**b**) NiO photocatalyst (Photocatalyst dosage = 2 mg L^{-1}, L-CHT = 20 mg L^{-1}). Initial pH: (■) pH = 5, (●) pH = 7, and (★) pH = 9.

Understanding the role of catalyst dosage on L-CHT degradation is of the utmost relevance to minimize the capital costs associated with the use of material. The objective should be to identify the lower dose of catalyst, which allows for higher removal at the fastest rate (low hydraulic retention time for continuous treatment). The effect of increasing photocatalyst concentration (CuO and NiO) on the photodegradation of L-CHT was studied by varying the photocatalyst dosage (1–5 mg L^{-1}) at a constant concentration of L-CHT (20 mg L^{-1}) and pH 7 (Figure 8). Figure 8 shows that, at a lower catalyst loading, the degradation of L-CHT is low because of the limited availability of catalytic sites that generate oxidants to degrade L-CHT. By using a CuO photocatalyst, the degradation efficiency of L-CHT was enhanced from 79% to 99% by increasing the amount of catalyst from 1 to 3 mg L^{-1}, and then decreased to 93% at 5 mg L^{-1}. Similar trends were observed when conducting degradation with a phyto-synthesized NiO photocatalyst. The degradation percentage of L-CHT attained was enhanced from 59% to 86% by increasing the amount of catalyst from 1 to 4 mg L^{-1}, and then decreased to 84% at 5 mg L^{-1}. The reason for the higher degradation rate is that more active sites are available with higher catalyst amounts given the larger surface area available for photocatalysts in solution. Hence, the enhanced production of electrons, holes and hydroxyl radicals leads to a higher degradation of L-CHT. However, additional increase in catalyst dosage beyond the optimum amount of catalyst results in a lower degradation. There are several reasons for the decrease in degradation capability under a higher catalyst dosage. First, high concentrations of the catalyst may lead to the blockage of photon penetration into the L-CHT solution [79,80]. A decrease in the efficiency of photon transport can diminish the photogeneration of charge carriers and oxidants in solution, therefore diminishing the degradation performance [81]. Second, the higher loading of nanoparticles can induce their agglomeration. The agglomeration of nanoparticles inhibits transport from/towards a solution to the catalyst surface and decreases the availability of active sites [82,83]. The lower interfacial surface results then in a lower abatement of target pollutant L-CHT, as observed for the higher dosages in Figure 8. Thus, 3 mg L^{-1} (CuO) and 4 mg L^{-1} (NiO) of catalysts were defined as the optimum dosage, which attains the highest removal with the lower mass addition.

Finally, it is important to understand the applicability of the phytochemical-synthesized catalysts on the treatment of a wide range of L-CHT concentrations. Figure 9 illustrates the removal of L-CHT at different initial concentrations, ranging from 10 to 70 mg L^{-1}, at the initial pH 7 and constant photocatalyst (2 mg L^{-1}). The photocatalytic degradation of L-CHT using a CuO photocatalyst was decreased from 99% to 79% when increasing the initial L-CHT concentration from 10 to 70 mg L^{-1} after 3 h. The photocatalytic degradation of

L-CHT using a NiO photocatalyst was decreased from 89% to nearly 68% with an increase in the initial L-CHT concentration from 10 to 70 mg L^{-1}. The decrease in the percentage of removal attained when increasing the concentration of target pollutant is associated with the fact that a higher number of molecules should react with the same number of oxidants that were generated by the identical number of catalytic sites. Furthermore, the presence of organic compounds that may absorb radiation can hinder photon transport and decrease at the same time as the generation rate of oxidants [84–86]. Despite the decrease in removal percentage attained at the same time as photocatalytic treatment, it can be deduced that the proposed photocatalysts can effectively degrade L-CHT within a wide range of environmental concentrations.

Figure 8. Effect of photocatalyst dosage ((■) 1 mg L^{-1}, (●) 2 mg L^{-1}, (★) 3 mg L^{-1}, (⬤) 4 mg L^{-1}, and (◆) 5 mg L^{-1}) on the photocatalytic degradation of L-CHT using (**a**) CuO, (**b**) NiO photocatalyst (Photocatalyst dosage = 1–5 mg L^{-1}, L-CHT = 20 mg L^{-1}, pH = 7).
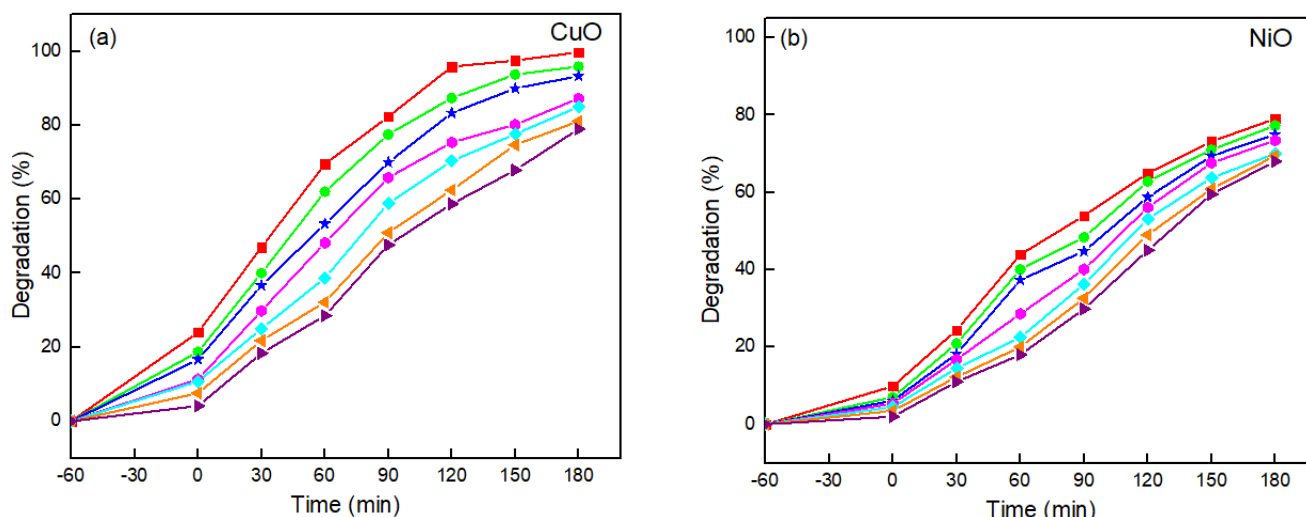
Figure 9. Effect of initial concentration of L-CHT ((■) 10 mg L^{-1}, (●) 20 mg L^{-1}, (★) 30 mg L^{-1}, (⬤) 40 mg L^{-1}, (◆) 50 mg L^{-1}, (▶) 60 mg L^{-1}, and (▲) 70 mg L^{-1} on the photocatalytic degradation of L-CHT using (**a**) CuO, (**b**) NiO photocatalyst (Photocatalyst dosage = 2 mg L^{-1}, L-CHT = 10–70 mg L^{-1}, pH = 7).

Our experimental results demonstrate effective abatement of L-CHT, but other by-product species may be formed during the treatment. The UV-vis spectra suggested a complete breakdown of aromatic rings, which may result in the yield of carboxylic acids

of low molecular weight. Furthermore, from the L-CHT structure, it is expected that the mineralization of this trace pollutant may yield small concentrations of fluoride, chloride, and nitrate. These species may be yielded from the heteroatoms of N, F, and Cl present in the L-CHT molecular structure. Further mechanistic studies to understand elemental steps in the degradation of L-CHT should be conducted to elucidate degradation pathways and the formation of by-products which are different from CO_2 and water as result of the organic pollutant mineralization.

2.4. Photocatalytic Stability of CuO and NiO Photocatalyst for Removal of L-CHT for Five Times

The prepared nanoparticles demonstrated high stability and recyclability during multiple photocatalytic cycles using fresh solutions containing L-CHT. Figure 10 shows the percentage of degradation attained by consecutive cycles. For recyclability, the photocatalysts after the degradation of L-CHT were collected by centrifugation and washed with distilled water and ethanol three times, and then regenerated catalysts were dried in a vacuum oven at 100 °C for 3 h.
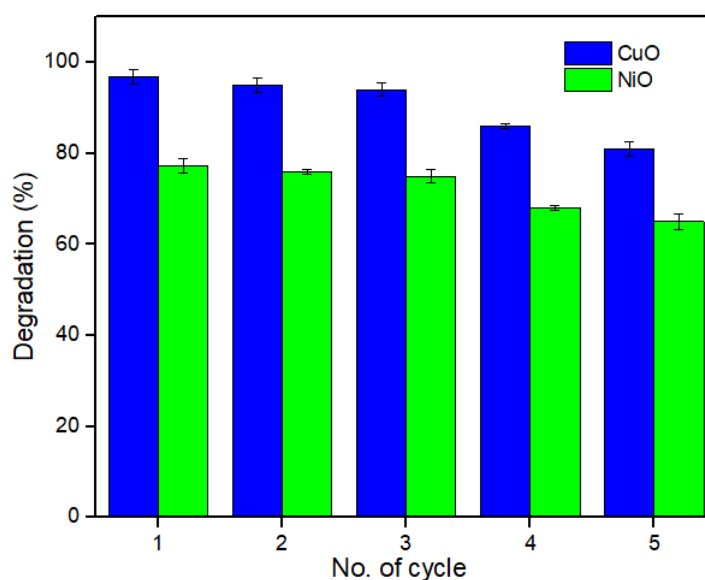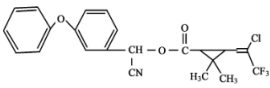

Figure 10. Reusability test of CuO and NiO photocatalysts upto five cycles against L-CHT.

3. Material and Methods

3.1. Chemicals

Analytical grade nickel nitrate, copper nitrate, sodium hydroxide, and ethanol were purchased from Sigma-Millipore. The pesticide L-CHT 95% pure was purchased from Ali Akbar group of industries, Lahore, Pakistan. The physico-chemical characteristics of L-CHT are given in Table 1. Commercial P25 TiO_2 from Degussa was used to benchmark the performance of synthesized catalysts. The *Capparis decidua* leaves were collected from the Jhang, Pakistan. The *Capparis decidua* leaves are a very competitive resource with a cost of ~20 USD kg^{-1}; however, it can be collected free of cost in Pakistan, where it grows naturally. In the past, *Capparis decidua* was used as food source and in natural medicinal applications, but, most recently, it is in disuse. Therefore, it can be considered an inexpensive natural resource, which is barely exploited. All chemical reagents were used without any further purification.

Table 1. Physico-chemical characteristics of pesticide lambda-cyhalothrin (L-CHT).

Pesticide	CAS Number	Molecular Weight	Formula	Structure
L-CHT	91465-08-6	449.9 g mol^{-1}	$C_{23}H_{19}ClF_3NO_3$	

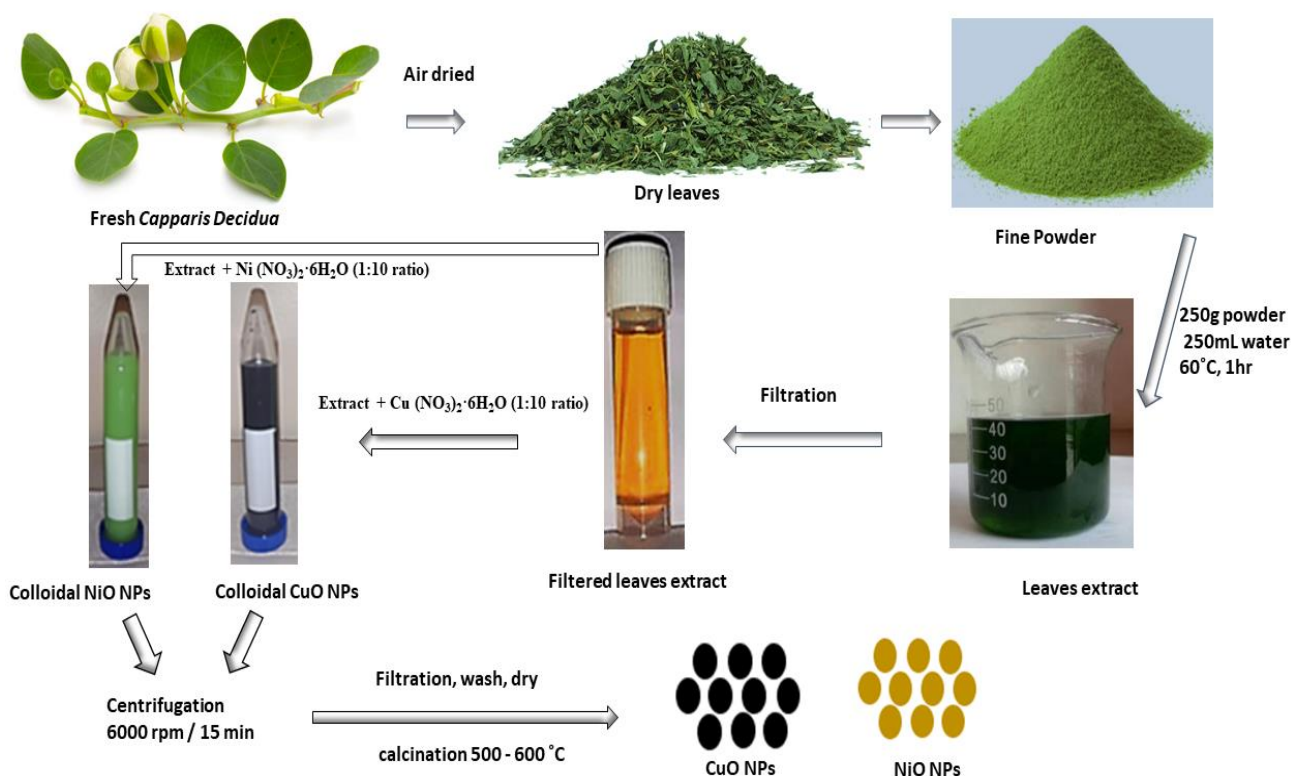### 3.2. Preparation of Plant Extract

Capparis decidua, commonly known as Karir, was extracted and used in the biosynthesis of CuO and NiO nanoparticles. The bioactive compounds with high antioxidant potential play an essential role as capping agents: flavonoids, saponins, steroids, tannins, and phenol. Figure 11 showed the phytochemicals present in *Capparis decidua* leaf extract [45]. The leaves of *Capparis decidua* were thoroughly washed with deionized water, then air-dried for 10–12 days to entirely remove water content. The dried leaves were then crushed to powder and preserved in an airtight container. The extract was obtained by dissolving 25 g of *Capparis decidua* fresh leaves powder with 250 mL distilled water. The mixture was heated for one hour at 60 °C under continuous stirring. The resulting solution was concentrated in a rotary evaporator and filtered thrice utilizing Whatman filter papers. The extract was then preserved at 4 °C for future use in the bio-fabrication of CuO and NiO nanoparticles.
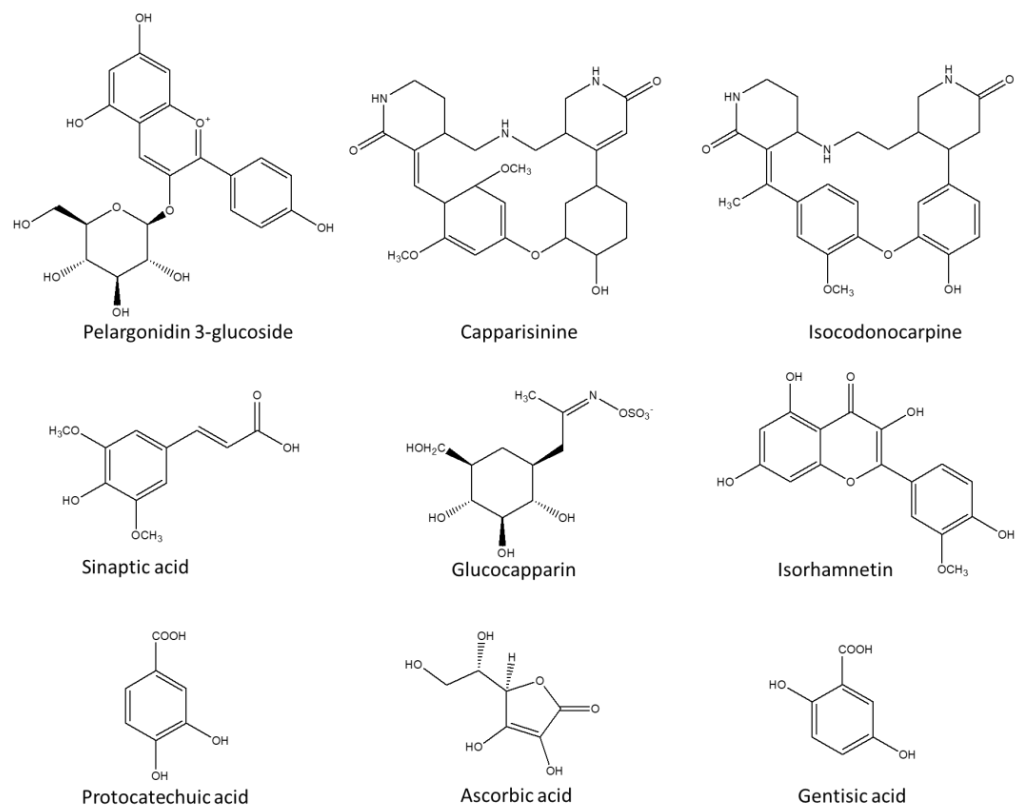
Figure 11. Reported phytochemicals present in *Capparis decidua* leaves extract.

3.3. Green synthesis of CuO and NiO Nanoparticles

To synthesize CuO nanoparticles, 200 mL solution of Cu (NO$_3$)$_2$·3H$_2$O in the concentration of 0.05mM was prepared in a 250 mL conical flask, and then add 20 mL of *Capparis decidua* aqueous extract (20 µg mL^{-1}). The proportion of of Cu (NO$_3$)$_2$·3H$_2$O solution and *Capparis decidua* aqueous extract was 1:10 for the green synthesis of CuO nanoparticles. To synthesize NiO nanoparticles, the same proportion of solutions was taken, but instead of adding 0.05 mM of 200 mL solution of Cu (NO$_3$)$_2$·3H$_2$O, 0.05 mM of 200 mL solution

of Ni $(NO_3)_2 \cdot 6H_2O$ was added. The resulting solution mixtures were allowed to react at room temperature under continuous stirring for 12 h to ensure a complete oxidation and reduction process. Initially, a color change was observed, which indicated the formation of CuO (dark yellow to dark green) and NiO (dark yellow to dark brown) nanoparticles. The obtained solutions at the end of the reaction were centrifuged at 6000 rpm for 15 min. The pallets containing CuO and NiO nanoparticles were carefully washed three times with double distilled water. The obtained pellets were then placed in the oven at 80 °C for 2 h. For effective crystallization, CuO and NiO nanoparticles were calcined in a muffle furnace for an hour at 600 °C and 500 °C, respectively. The calcination conditions were based on previous reports [87,88]. The calcined CuO (black color powder) and NiO (light yellow powder) nanoparticles were kept in a dry container until use. Figure 12 shows the color differences in the materials.

Figure 12. Schematic depiction of preparation of CuO and ZnO NPs using *Capparis decidua* leaves extract.

3.4. Photocatalytic Degradation Experiments

The photocatalytic degradation of L-CHT as a contaminant using green synthesized CuO and NiO NPs was carried out under ultraviolet light irradiation. The L-CHT was first dissolved in 10 mL of methanol to prepare a 500 mg L^{-1} stock solution and stored at 4 °C without light. Working standards were prepared by diluting the stock solution in ultrapure water. Experimental solutions of 10 mg L^{-1} to 70 mg L^{-1} of L-CHT contained 1.0% methanol. Given the reactive oxygen species (ROS) scavenging character of organic alcohols, methanol may consume some photogenerated oxidants, which compete during L-CHT degradation. Therefore, the reported kinetic constants are conservative (i.e., the lower bound of what would occur in natural waters without elevated levels of ROS scavengers). The photocatalytic degradation experiments were carried out in a closed, box reactor containing 8×18 W UV lamps (ZamZam micro technologies ZM 144W, $\lambda_{max} = 254$ nm) at room temperature. The intensity of UV irradiations was measured using a UV radiometer (UVX digital radiometer, Analytic Jena, with probe UVX-25 probe for 254 nm light). To maintain constant light intensity, the distance between the UV light source lamp and test solution was kept at 10 cm above the solution reactor. Experiments were conducted using

150 mL of solution. To attain an adsorption/desorption equilibrium between nanocatalyst and pesticide solution, the obtained suspension was kept in dark conditions and stirred for 1 h at constant temperature (25 °C). For enhanced degradation of L-CHT, different parameters were optimized. The desired amount of nanocatalyst was added (1–5 mg L^{-1}) to the L-CHT solution with different concentrations (10–70 mg L^{-1}) at a certain pH (5–9), and the contact time for irritation was 3 h. Aliquots of 3 mL were collected at a regular time interval for 3 h after irritation, and then centrifuged at 4000 rpm for 10 min to remove the photocatalyst from L-CHT. All experiments were conducted in triplicate and showed high reproducibility, with an estimated error of below 5%. The concentration of L-CHT was estimated through UV-vis measurements. The percentage (%) degradation was calculated using Equation (2):

$$\text{Degradation (\%)} = \frac{C_0 - C}{C_0} \times 100, \tag{2}$$

where C_0 and C refer to the initial and final concentrations of L-CHT, respectively.

3.5. Characterization Methods and Instruments

The synthesized CuO and NiO nanoparticles were characterized using solid-state techniques. The reduction in metal oxide nanoparticles was determined by measuring ultraviolet-visible (UV-vis) absorption spectra recorded using UV-4000 UV-Vis spectrophotometer (Hamburg, Germany). A Field-Emission-Scanning electron microscope (FE-SEM, QUANTAFEG 250, Eindhoven, The Netherlands) was used to study the morphological properties, in terms of their size and shape. Fourier Transform Infrared spectrometer (Bruker ALPHA) at a scanning range of 400 to 4000 cm^{-1} wavelength was used for the identification of functional groups involved in the reduction in nanoparticles. Elemental compositions of nanoparticles were analyzed using Energy-Dispersive X-ray (EDX-INCA 200 Oxford Instruments, High Wycombe, UK). Thermogravimetric Analysis and Differential Scanning Calorimetry (TGA-DTA; STA 1500 Rheometric Scientific (Surrey, UK)) at a heating rate of 10 °C min^{-1} in air within a temperature range of from 30 °C to 800 °C.

4. Conclusions

A simple, rapid, and environmentally friendly procedure is adopted to prepare stable CuO and NiO nanoparticles using *Capparis decidua* leaf extract. Their effectiveness was evaluated from the degradation of L-CHT pesticide in aqueous solutions. The prepared nanoparticles were characterized by UV-vis, FE-SEM, EDX, XRD, TGA/DTA, and FTIR. The flower and spherical shape morphology of nanoparticles was confirmed by FESEM. The XRD pattern confirmed the face-centered cubic structure of CuO and NiO nanoparticles, with an average crystallite size of 11.23 and 16.75 nm, respectively. The *Capparis decidua* leaf extracts contain various phytochemicals, such as phenols, ascorbic acid, flavonoids, polyphenolic, citric acid, alkaloids, etc. These biologically active compounds act as reducing and stabilizing agents, which help in the reduction in metal ion precursors. A comparative photocatalytic activity study was conducted for the CuO and NiO nanoparticles. The results showed that CuO (99%) exhibited a higher photocatalytic activity than NiO (89%), although NiO demonstrated a higher stability in the long-term. A comparison of the photocatalytic removal of CuO and NiO photocatalyst showed that the removal of L-CHT is faster using a CuO compared to NiO photocatalyst, and that both catalysts are promising, inexpensive and sustainable alternatives for water treatment.

Author Contributions: Conceptualization, A.I., A.u.H., S.A.R.N., P.W., and S.G.-S.; methodology, A.I., A.u.H., G.A.C.-C., S.A.R.N., P.W., and S.G.-S.; validation, A.u.H., G.A.C.-C., S.A.R.N. and A.I.; formal analysis, A.I.; investigation, A.I., G.A.C.-C.; resources, S.A.R.N., P.W., S.G.-S.; data curation, A.I.; writing—original draft preparation, A.I., S.G.-S.; writing—review and editing, A.I., G.A.C.-C., S.G.-S., P.W.; visualization, A.I., S.G.-S.; supervision, A.u.H., S.A.R.N., S.G.-S.; project administration, P.W.; funding acquisition, A.u.H., S.A.R.N., P.W., S.G.-S. All authors have read and agreed to the published version of the manuscript.

References

1. Bolzonella, C.; Lucchetta, M.; Teo, G.; Boatto, V.; Zanella, A. Is there a way to rate insecticides that is less detrimental to human and environmental health? *Glob. Ecol. Conserv.* **2019**, *20*, e00699. [CrossRef]
2. Wang, Q.; Rao, P.; Li, G.; Dong, L.; Zhang, X.; Shao, Y.; Gao, N.; Chu, W.; Xu, B.; An, N.; et al. Degradation of imidacloprid by UV-activated persulfate and peroxymonosulfate processes: Kinetics, impact of key factors and degradation pathway. *Ecotoxicol. Environ. Saf.* **2020**, *187*, 109779. [CrossRef] [PubMed]
3. Heck, K.N.; Garcia-Segura, S.; Westerhoff, P.; Wong, M.S. Catalytic Converters for Water Treatment. *Accounts Chem. Res.* **2019**, *52*, 906–915. [CrossRef] [PubMed]
4. Tudi, M.; Ruan, H.D.; Wang, L.; Lyu, J.; Sadler, R.; Connell, D.; Chu, C.; Phung, D. Agriculture Development, Pesticide Application and Its Impact on the Environment. *Int. J. Environ. Res. Public Health* **2021**, *18*, 1112. [CrossRef] [PubMed]
5. Capodaglio, A.G. Integrated, Decentralized Wastewater Management for Resource Recovery in Rural and Peri-Urban Areas. *Resour.* **2017**, *6*, 22. [CrossRef]
6. Zulfikar, M.; Nadeem, R.; Javed, T.; Jilani, M.I.; Javed, I. Green synthesis of Fe nanoparticles by using Mangifera indica extract and its application in photo-catalytic degradation of dyes. *Water Sci. Technol.* **2021**, *83*, 1739–1752. [CrossRef]
7. Huang, Y.; Xiao, L.; Li, F.; Xiao, M.; Lin, D.; Long, X.; Wu, Z. Microbial Degradation of Pesticide Residues and an Emphasis on the Degradation of Cypermethrin and 3-phenoxy Benzoic Acid: A Review. *Molecules* **2018**, *23*, 2313. [CrossRef]
8. Gómez-Pastora, J.; Dominguez, S.; Bringas, E.; Rivero, M.J.; Ortiz, I.; Dionysiou, D. Review and perspectives on the use of magnetic nanophotocatalysts (MNPCs) in water treatment. *Chem. Eng. J.* **2017**, *310*, 407–427. [CrossRef]
9. Rueda-Marquez, J.J.; Levchuk, I.; Fernández Ibañez, P.; Sillanpää, M. A critical review on application of photocatalysis for toxicity reduction of real wastewaters. *J. Clean. Prod.* **2020**, *258*, 120694. [CrossRef]
10. Venieri, D.; Mantzavinos, D.; Binas, V. Solar Photocatalysis for Emerging Micro-Pollutants Abatement and Water Disinfection: A Mini-Review. *Sustainability* **2020**, *12*, 10047. [CrossRef]
11. Oliveros, A.N.; Pimentel, J.A.I.; de Luna, M.D.G.; Garcia-Segura, S.; Abarca, R.R.M.; Doong, R.-A. Visible-light photocatalytic diclofenac removal by tunable vanadium pentoxide/boron-doped graphitic carbon nitride composite. *Chem. Eng. J.* **2021**, *403*, 126213. [CrossRef]
12. Cuerda-Correa, E.M.; Alexandre-Franco, M.F.; Fernández-González, C. Advanced Oxidation Processes for the Removal of Antibiotics from Water. An Overview. *Water* **2020**, *12*, 102. [CrossRef]
13. Tugaoen, H.O.; Garcia-Segura, S.; Hristovski, K.; Westerhoff, P. Compact light-emitting diode optical fiber immobilized TiO2 reactor for photocatalytic water treatment. *Sci. Total Environ.* **2018**, *613–614*, 1331–1338. [CrossRef]
14. Fagan, R.; McCormack, D.E.; Dionysiou, D.D.; Pillai, S.C. A review of solar and visible light active TiO2 photocatalysis for treating bacteria, cyanotoxins and contaminants of emerging concern. *Mater. Sci. Semicond. Process.* **2016**, *42*, 2–14. [CrossRef]
15. Monteiro, R.A.; Miranda, S.; Vilar, V.; Pastrana-Martínez, L.M.; Tavares, P.; Boaventura, R.A.; Faria, J.L.; Pinto, E.; Silva, A.M. N-modified TiO 2 photocatalytic activity towards diphenhydramine degradation and Escherichia coli inactivation in aqueous solutions. *Appl. Catal. B Environ.* **2015**, *162*, 66–74. [CrossRef]
16. Villaluz, F.J.A.; de Luna, M.D.G.; Colades, J.I.; Garcia-Segura, S.; Lu, M.-C. Removal of 4-chlorophenol by visible-light photocatalysis using ammonium iron(II) sulfate-doped nano-titania. *Process. Saf. Environ. Prot.* **2019**, *125*, 121–128. [CrossRef]
17. EL-Sheshtawy, H.S.; El-Hosainy, H.M.; Shoueir, K.R.; El-Mehasseb, I.M.; El-Kemary, M. Facile immobilization of Ag nano-particles on g-C3N4/V2O5 surface for enhancement of post-illumination, catalytic, and photocatalytic activity removal of organic and inorganic pollutants. *Appl. Surf. Sci.* **2019**, *467–468*, 268–276. [CrossRef]
18. Chen, J.; Loeb, S.; Kim, J.-H. LED revolution: Fundamentals and prospects for UV disinfection applications. *Environ. Sci. Water Res. Technol.* **2017**, *3*, 188–202. [CrossRef]
19. Brillas, E.; Serrà, A.; Garcia-Segura, S. Biomimicry designs for photoelectrochemical systems: Strategies to improve light delivery efficiency. *Curr. Opin. Electrochem.* **2021**, *26*, 100660. [CrossRef]
20. Batista, L.M.B.; dos Santos, A.J.; da Silva, D.R.; Alves, A.P.D.M.; Garcia-Segura, S.; Martínez-Huitle, C.A. Solar photocatalytic application of NbO 2 OH as alternative photocatalyst for water treatment. *Sci. Total Environ.* **2017**, *596–597*, 79–86. [CrossRef]
21. Dos Santos, A.J.; Batista, L.M.B.; Martínez-Huitle, C.A.; Alves, A.P.D.M.; Garcia-Segura, S. Niobium Oxide Catalysts as Emerging Material for Textile Wastewater Reuse: Photocatalytic Decolorization of Azo Dyes. *Catalysts* **2019**, *9*, 1070. [CrossRef]
22. Sabouri, Z.; Akbari, A.; Hosseini, H.A.; Darroudi, M. Facile green synthesis of NiO nanoparticles and investigation of dye degradation and cytotoxicity effects. *J. Mol. Struct.* **2018**, *1173*, 931–936. [CrossRef]

23. Yu, C.; Wen, M.; Tong, Z.; Li, S.; Yin, Y.; Liu, X.; Li, Y.; Liang, T.; Wu, Z.; Dionysiou, D.D. Synthesis and enhanced photo-catalytic performance of 0D/2D CuO/tourmaline composite photocatalysts. *Beilstein J. Nanotechnol.* **2020**, *11*, 407–416. [CrossRef]

24. Yu, X.; Zhang, J.; Zhao, Z.; Guo, W.; Qiu, J.; Mou, X.; Li, A.; Claverie, J.P.; Liu, H. NiO-TiO2 p-n heterostructured nanocables bridged by zero-bandgap rGO for highly efficient photocatalytic water splitting. *Nano Energy* **2015**, *16*, 207–217. [CrossRef]

25. Dhineshbabu, N.R.; Rajendran, V.; Nithyavathy, N.; Vetumperumal, R. Study of structural and optical properties of cupric oxide nanoparticles. *Appl. Nanosci.* **2015**, *6*, 933–939. [CrossRef]

26. Serrà, A.; Philippe, L.; Perreault, F.; Garcia-Segura, S. Photocatalytic treatment of natural waters. Reality or hype? The case of cyanotoxins remediation. *Water Res.* **2021**, *188*, 116543. [CrossRef]

27. Gonçalves, R.; Toledo, R.; Joshi, N.; Berengue, O. Green Synthesis and Applications of ZnO and TiO$_2$ Nanostructures. *Molecules* **2021**, *26*, 2236. [CrossRef] [PubMed]

28. Mondejar, M.E.; Avtar, R.; Diaz, H.L.B.; Dubey, R.K.; Esteban, J.; Gomez-Morales, A.; Hallam, B.; Mbungi, N.T.; Okolo, C.C.; Prasad, K.A.; et al. Digitalization to achieve sustainable development goals: Steps towards a Smart Green Plane. *Sci. Total Environ.* **2021**, 148539. [CrossRef]

29. Tugaoen, H.; Garcia-Segura, S.; Hristovski, K.; Westerhoff, P. Challenges in photocatalytic reduction of nitrate as a water treatment technology. *Sci. Total Environ.* **2017**, *599–600*, 1524–1551. [CrossRef]

30. Akel, S.; Dillert, R.; Balayeva, N.O.; Boughaled, R.; Koch, J.; El Azzouzi, M.; Bahnemann, D.W. Ag/Ag2O as a Co-Catalyst in TiO2 Photocatalysis: Effect of the Co-Catalyst/Photocatalyst Mass Ratio. *Catalysts* **2018**, *8*, 647. [CrossRef]

31. Aljabali, A.A.A.; Akkam, Y.; Al Zoubi, M.S.; Al-Batayneh, K.M.; Al-Trad, B.; Alrob, O.A.; Alkilany, A.M.; Benamara, M.; Evans, D.J. Synthesis of Gold Nanoparticles Using Leaf Extract of Ziziphus zizyphus and their Antimicrobial Activity. *Nanomaterials* **2018**, *8*, 174. [CrossRef]

32. Khan, S.H.; Pathak, B. Zinc oxide based photocatalytic degradation of persistent pesticides: A comprehensive review. *Environ. Nanotechnol. Monit. Manag.* **2020**, *13*, 100290. [CrossRef]

33. Serrà, A.; Gómez, E.; Philippe, L. Bioinspired ZnO-based solar photocatalysts for the efficient decontamination of persistent organic pollutants and hexavalent chromium in wastewater. *Catalysts* **2019**, *9*, 974. [CrossRef]

34. Wang, Y.; O'Connor, D.; Shen, Z.; Lo, I.M.; Tsang, D.; Pehkonen, S.; Pu, S.; Hou, D. Green synthesis of nanoparticles for the remediation of contaminated waters and soils: Constituents, synthesizing methods, and influencing factors. *J. Clean. Prod.* **2019**, *226*, 540–549. [CrossRef]

35. Varghese, J.; Zikalala, N.; Sakho, E.H.M.; Oluwafemi, O.S. *Green Synthesis Protocol on Metal Oxide Nanoparticles Using Plant Extracts*; Elsevier BV, 2020; pp. 67–82. Available online: https://www.sciencedirect.com/science/article/pii/B9780128133576000061?via%3Dihub (accessed on 22 June 2021).

36. Yahia, Y.; Benabderrahim, M.A.; Tlili, N.; Bagues, M.; Nagaz, K. Bioactive compounds, antioxidant and antimicrobial activities of extracts from different plant parts of two Ziziphus Mill. species. *PLoS ONE* **2020**, *15*, e0232599. [CrossRef] [PubMed]

37. Kumar, H.; Bhardwaj, K.; Kuča, K.; Kalia, A.; Nepovimova, E.; Verma, R.; Kumar, D. Flower-Based Green Synthesis of Metallic Nanoparticles: Applications beyond Fragrance. *Nanomaterials* **2020**, *10*, 766. [CrossRef]

38. Sarkar, J.; Chakraborty, N.; Chatterjee, A.; Bhattacharjee, A.; Dasgupta, D.; Acharya, K. Green Synthesized Copper Oxide Nanoparticles Ameliorate Defence and Antioxidant Enzymes in Lens culinaris. *Nanomaterials* **2020**, *10*, 312. [CrossRef] [PubMed]

39. Chowdhury, R.; Khan, A.; Rashid, H. Green synthesis of CuO nanoparticles using Lantana camara flower extract and their potential catalytic activity towards the aza-Michael reaction. *RSC Adv.* **2020**, *10*, 14374–14385. [CrossRef]

40. Sukumar, S.; Rudrasenan, A.; Padmanabhan Nambiar, D. Green-aynthesized rice-shaped copper oxide nanoparticles using Caesalpinia bonducella seed extract and their applications. *ACS Omega* **2020**, *5*, 1040–1051. [CrossRef] [PubMed]

41. Olajire, A.; Mohammed, A. Green synthesis of nickel oxide nanoparticles and studies of their photocatalytic activity in degradation of polyethylene films. *Adv. Powder Technol.* **2020**, *31*, 211–218. [CrossRef]

42. Zhang, Y.; Mahdavi, B.; Mohammadhosseini, M.; Rezaei-Seresht, E.; Paydarfard, S.; Qorbani, M.; Karimian, M.; Abbasi, N.; Ghaneialvar, H.; Karimi, E. Green synthesis of NiO nanoparticles using Calendula officinalis extract: Chemical charactrization, antioxidant, cytotoxicity, and anti-esophageal carcinoma properties. *Arab. J. Chem.* **2021**, *14*, 103105. [CrossRef]

43. Boudiaf, M.; Messai, Y.; Bentouhami, E.; Schmutz, M.; Blanck, C.; Ruhlmann, L.; Bezzi, H.; Tairi, L.; Mekki, D.E. Green synthesis of NiO nanoparticles using Nigella sativa extract and their enhanced electro-catalytic activity for the 4-nitrophenol degradation. *J. Phys. Chem. Solids* **2021**, *153*, 110020. [CrossRef]

44. Dhakad, P.K.; Sharma, P.K.; Kumar, S. A Review on Ethnobiological & Medicinal Potential of Capparaceae Family Plant: Capparis decidua (Forssk.) Edgew. *Adv. Pharmacol. Pharm.* **2016**, *4*, 27–39. [CrossRef]

45. Nazar, S.; Hussain, M.A.; Khan, A.; Muhammad, G.; Tahir, M.N. Capparis decidua Edgew (Forssk.): A comprehensive review of its traditional uses, phytochemistry, pharmacology and nutrapharmaceutical potential. *Arab. J. Chem.* **2020**, *13*, 1901–1916. [CrossRef]

46. Iqbal, A.; Anwar, F.; Nadeem, R.; Sultana, B.; Mushtaq, M. Proximate Composition and Minerals Profile of Fruit and Flower of Karir (Capparis decidua) from Different Regions of Punjab (Pakistan). *Asian J. Chem.* **2014**, *26*, 360–364. [CrossRef]

47. Raza, M.A.; Younas, M.; Schlecht, E. In vitro efficacy of selected medicinal plants from Cholistan desert, Pakistan, against gastrointestinal helminths of sheep and goats. *J. Agric. Rural Dev. Trop. Subtrop.* **2016**, *117*, 211–224.

48. Khan, M.I.; Shoukat, M.A.; Cheema, S.A.; Arif, H.N.; Niazi, N.K.; Azam, M.; Bashir, S.; Ashraf, I.; Qadri, R. Use, contami-nation and exposure of pesticides in pakistan: A review. *Pak. J. Agric. Sci.* **2020**, *57*, 131–149.

49. Ghumro, W.A.; Phulpoto, A.H.; Qazi, M.A.; Mangi, S.; Pirzada, T.; Ahmed, S.; Kanhar, N.A. Pesticide Lambda-Cyhalothrin degradation using Mesorhizobium sp. (S1b) and Bartonella sp. (S2b) strains isolated from cotton crop. *Pak. J. Anal. Environ. Chem.* **2017**, *18*, 112–119. [CrossRef]

50. Saleem, U.; Ejaz, S.; Ashraf, M.; Omer, M.O.; Altaf, I.; Batool, Z.; Fatima, R.; Afzal, M. Mutagenic and cytotoxic potential of Endosulfan and Lambda-cyhalothrin—In vitro study describing individual and combined effects of pesticides. *J. Environ. Sci.* **2014**, *26*, 1471–1479. [CrossRef]

51. Nieradko-Iwanicka, B.; Konopelko, M. Effect of Lambdacyhalothrin on Locomotor Activity, Memory, Selected Biochemical Parameters, Tumor Necrosis Factor α, and Interleukin 1ß in a Mouse Model. *Int. J. Environ. Res. Public Health* **2020**, *17*, 9240. [CrossRef]

52. Bownik, A.; Kowalczyk, M.; Bańczerowski, J. Lambda-cyhalothrin affects swimming activity and physiological responses of Daphnia magna. *Chemosphere* **2019**, *216*, 805–811. [CrossRef] [PubMed]

53. Sahu, D.K.; Rai, J.; Bhatt, C.; Rai, M.K.; Goswami, J.; Sahu, A.K.; Singh, T.V.; Nirmala, M.; Mundeja, K.W.A.P. UV-Visible Spectrophotometric Determination of Lambda-Cyhalothrin Insecticide in Vegetables, Soil and Water Samples. *J. Ravishankar Univ. (Part-B)* **2018**, *31*, 1–9. [CrossRef]

54. Shahzadi, N.; Imran, M.; Sarwar, M.; Hashmi, A.S. Identification of pesticides residues in different samples of milk. *J. Agroaliment. Process. Technol.* **2013**, *19*, 167–172.

55. Li, H.; Fang, Y.; Ni, C.; Chen, X.; Mo, J.; Lv, Y.; Chen, Y.; Chen, X.; Lian, Q.; Ge, R.-S. Lambda-cyhalothrin delays pubertal Leydig cell development in rats. *Environ. Pollut.* **2018**, *242*, 709–717. [CrossRef] [PubMed]

56. Shen, W.; Lou, B.; Xu, C.; Yang, G.; Yu, R.; Wang, X.; Li, X.; Wang, Q.; Wang, Y. Lethal toxicity and gene expression changes in embryonic zebrafish upon exposure to individual and mixture of malathion, chlorpyrifos and lambda-cyhalothrin. *Chemosphere* **2020**, *239*, 124802. [CrossRef] [PubMed]

57. Al-Amoudi, W.M. Toxic effects of Lambda-cyhalothrin, on the rat thyroid: Involvement of oxidative stress and ameliorative effect of ginger extract. *Toxicol. Rep.* **2018**, *5*, 728–736. [CrossRef]

58. Liao, C.H.; He, X.J.; Wang, Z.L.; Barron, A.B.; Zhang, B.; Zeng, Z.J.; Wu, X.B. Short-Term Exposure to Lamb-da-Cyhalothrin Negatively Affects the Survival and Memory-Related Characteristics of Worker Bees Apis mellifera. *Arch. Environ. Contam. Toxicol.* **2018**, *75*, 59–65. [CrossRef] [PubMed]

59. Ezenwosu, S.U.; Nnamonu, E.I.; Odo, G.E.; Ikele, B.C.; Ani, O.C. Evaluation of lambda-cyhalothrin oxidative stress and gonad histoarchitecture toxicity potency in Clarias gariepinus. *J. Basic Appl. Zool.* **2021**, *82*, 1–11. [CrossRef]

60. Fetoui, H.; Makni, M.; Garoui, E.M.; Zeghal, N. Toxic effects of lambda-cyhalothrin, a synthetic pyrethroid pesticide, on the rat kidney: Involvement of oxidative stress and protective role of ascorbic acid. *Exp. Toxicol. Pathol.* **2010**, *62*, 593–599. [CrossRef]

61. Verma, J.P.; Jaiswal, D.K.; Sagar, R. Pesticide relevance and their microbial degradation: A-state-of-art. *Rev. Environ. Sci. Bio/Technol.* **2014**, *13*, 429–466. [CrossRef]

62. Al-Sarar, A.S.; Abobakr, Y.; Bayoumi, A.E.; Hussein, H.I.; Al-Ghothemi, M. Reproductive toxicity and histopathological changes induced by lambda-cyhalothrin in male mice. *Environ. Toxicol.* **2012**, *29*, 750–762. [CrossRef]

63. Ministry of the Environment of Canada. Class 9 Pesticide Ingredients Banned for Cosmetic Use as Classified by the Ontario, Canada, Ministry of the Environment. 2013. Available online: https://www.beyondpesticides.org/assets/media/documents/lawn/documents/Class9PesticideIngredientsBannedforCosmeticUseasClassifiedbytheOntario-FINAL.pdf (accessed on 29 June 2021).

64. *EPA Lambda-Cyhalothrin; Receipt of Application for Emergency Exemption, Solicitation of Public Comment*; Environmental Protection Agency: Washington, DC, USA, 2020; Volume 85.

65. Chaudhary, S.; Kaur, Y.; Jayee, B.; Chaudhary, G.R.; Umar, A. NiO nanodisks: Highly efficient visible-light driven photocatalyst, potential scaffold for seed germination of Vigna Radiata and antibacterial properties. *J. Clean. Prod.* **2018**, *190*, 563–576. [CrossRef]

66. Saravanan, S.; Sivasankar, T. Effect of ultrasound power and calcination temperature on the sonochemical synthesis of copper oxide nanoparticles for textile dyes treatment. *Environ. Prog. Sustain. Energy* **2016**, *35*, 669–679. [CrossRef]

67. Bharathi, D.; Preethi, S.; Abarna, K.; Nithyasri, M.; Kishore, P.; Deepika, K. Bio-inspired synthesis of flower shaped iron oxide nanoparticles (FeONPs) using phytochemicals of Solanum lycopersicum leaf extract for biomedical applications. *Biocatal. Agric. Biotechnol.* **2020**, *27*, 101698. [CrossRef]

68. Lalithambika, K.C.; Thayumanavan, A.; Ravichandran, K.; Sriram, S. Photocatalytic and antibacterial activities of eco-friendly green synthesized ZnO and NiO nanoparticles. *J. Mater. Sci. Mater. Electron.* **2017**, *28*, 2062–2068. [CrossRef]

69. Arya, A.; Gupta, K.; Chundawat, T.S.; Vaya, D. Biogenic synthesis of copper and silver nanoparticles using green alga Botryococcus braunii and its antimicrobial activity. *Bioinorg. Chem. Appl.* **2018**, *2018*, 789403. [CrossRef] [PubMed]

70. Shashanka, R. Investigation of optical and thermal properties of CuO and ZnO nanoparticles prepared by Crocus Sativus (Saffron) flower extract. *J. Iran. Chem. Soc.* **2021**, *18*, 415–427. [CrossRef]

71. Mayedwa, N.; Mongwaketsi, N.; Khamlich, S.; Kaviyarasu, K.; Matinise, N.; Maaza, M. Green synthesis of nickel oxide, palladium and palladium oxide synthesized via Aspalathus linearis natural extracts: Physical properties & mechanism of for-mation. *Appl. Surf. Sci.* **2018**, *446*, 266–272.

72. Ezhilarasi, A.A.; Vijaya, J.J.; Kaviyarasu, K.; Maaza, M.; Ayeshamariam, A.; Kennedy, L.J. Green synthesis of NiO nanopar-ticles using Moringa oleifera extract and their biomedical applications: Cytotoxicity effect of nanoparticles against HT-29 cancer cells. *J. Photochem. Photobiol. B Biol.* **2016**, *164*, 352–360. [CrossRef]

73. Philip, D. Green synthesis of gold and silver nanoparticles using Hibiscus rosa sinensis. *Phys. E Low-Dimens. Syst. Nanostruct.* **2010**, *42*, 1417–1424. [CrossRef]

74. Narayan, H.; Alemu, H.; Jaybhaye, S. Copper Oxide Nanoparticles: Synthesis and Characterization. In Proceedings of the AATMC-2018, Kalyan, India, 28 February 2018; pp. 43–47.

75. Sorbiun, M.; Shayegan Mehr, E.; Ramazani, A.; Taghavi Fardood, S. Green synthesis of zinc oxide and copper oxide nano-particles using aqueous extract of oak fruit hull (Jaft) and comparing their photocatalytic degradation of Basic Violet 3. *Int. J. Environ. Res.* **2018**, *12*, 29–37. [CrossRef]

76. Sudhasree, S.; Banu, A.S.; Brindha, P.; Kurian, G.A. Synthesis of nickel nanoparticles by chemical and green route and their comparison in respect to biological effect and toxicity. *Toxicol. Environ. Chem.* **2014**, *96*, 743–754. [CrossRef]

77. Prabhu, V.G.; Shajira, P.; Lakshmi, N.; Bushiri, M.J. Magnetic properties of Ni/NiO nanocomposites synthesized by one step solution combustion method. *J. Phys. Chem. Solids* **2015**, *87*, 238–243. [CrossRef]

78. Pillai, S.C.; Štangar, U.L.; Byrne, J.A.; Pérez-Larios, A.; Dionysiou, D.D. Photocatalysis for disinfection and removal of contaminants of emerging concern. *Chem. Eng. J.* **2015**, *261*, 1–2. [CrossRef]

79. Marcelino, R.; Amorim, C.C. Towards visible-light photocatalysis for environmental applications: Band-gap engineering versus photons absorption—A review. *Environ. Sci. Pollut. Res.* **2018**, *26*, 4155–4170. [CrossRef] [PubMed]

80. Koppenol, W.H.; Stanbury, D.M.; Bounds, P.L. Electrode potentials of partially reduced oxygen species, from dioxygen to water. *Free. Radic. Biol. Med.* **2010**, *49*, 317–322. [CrossRef]

81. Deng, F.; Zhang, Q.; Yang, L.; Luo, X.; Wang, A.; Luo, S.; Dionysiou, D. Visible-light-responsive graphene-functionalized Bi-bridge Z-scheme black BiOCl/Bi2O3 heterojunction with oxygen vacancy and multiple charge transfer channels for efficient photocatalytic degradation of 2-nitrophenol and industrial wastewater treatment. *Appl. Catal. B Environ.* **2018**, *238*, 61–69. [CrossRef]

82. Zangeneh, H.; Zinatizadeh, A.A.; Feyzi, M.; Zinadini, S.; Bahnemann, D.W. Photomineralization of recalcitrant wastewaters by a novel magnetically recyclable boron doped-TiO2-SiO2 cobalt ferrite nanocomposite as a visible-driven heterogeneous photocatalyst. *J. Environ. Chem. Eng.* **2018**, *6*, 6370–6381. [CrossRef]

83. Marinho, B.A.; Cristóvão, R.O.; Djellabi, R.; Caseiro, A.; Miranda, S.M.; Loureiro, J.M.; Boaventura, R.A.; Dias, M.; Lopes, J.C.B.; Vilar, V.J. Strategies to reduce mass and photons transfer limitations in heterogeneous photocatalytic processes: Hexavalent chromium reduction studies. *J. Environ. Manag.* **2018**, *217*, 555–564. [CrossRef] [PubMed]

84. Khedr, T.M.; El-Sheikh, S.M.; Hakki, A.; Ismail, A.A.; Badawy, W.A.; Bahnemann, D.W. Highly active non-metals doped mixed-phase TiO 2 for photocatalytic oxidation of ibuprofen under visible light. *J. Photochem. Photobiol. A Chem.* **2017**, *346*, 530–540. [CrossRef]

85. Khan, S.; Han, C.; Sayed, M.; Sohail, M.; Jan, S.; Sultana, S.; Khan, H.M.; Dionysiou, D.D. Exhaustive Photocatalytic Lindane Degradation by Combined Simulated Solar Light-Activated Nanocrystalline TiO$_2$ and Inorganic Oxidants. *Catalysts* **2019**, *9*, 425. [CrossRef]

86. Díez, A.M.; Moreira, F.C.; Marinho, B.A.; Espindola, J.; Paulista, L.O.; Sanromán, M.; Pazos, M.; Boaventura, R.A.; Vilar, V.J. A step forward in heterogeneous photocatalysis: Process intensification by using a static mixer as catalyst support. *Chem. Eng. J.* **2018**, *343*, 597–606. [CrossRef]

87. Premalatha, N.; Miranda, L.R. Surfactant modified ZnO–Bi2O3 nanocomposite for degradation of lambda- cyhalothrin pesticide in visible light: A study of reaction kinetics and intermediates. *J. Environ. Manag.* **2019**, *246*, 259–266. [CrossRef]

88. Jonidi-Jafari, A.; Shirzad-Siboni, M.; Yang, J.K.; Naimi-Joubani, M.; Farrokhi, M. Photocatalytic degradation of diazinon with illuminated ZnO-TiO2 composite. *J. Taiwan Inst. Chem. Eng.* **2015**, *50*, 100–107. [CrossRef]